Dynamic Characterization of the Crew Module Uprighting System for NASA's Orion Crew Module

Ivan Rodrigues Bertaska
Marshall Space Flight Center
National Aeronautics and Space Administration
Huntsville, AL, USA
ivan.r.bertaska@nasa.gov

Tannen VanZwieten
Langley Research Center
National Aeronautics and Space Administration
Hampton, VA, USA
tannen.s.vanzwieten@nasa.gov

Jennifer Mann
Applied Physics Lab
Johns Hopkins University
Laurel, MD, USA
jennifer.mann@jhuapl.edu

Benjamin Connell
Applied Phyiscal Sciences
Groton, CT, USA
bconnell@aphysci.com

Tara Radke
Johnson Space Center
National Aeronautics and Space Administration
Houston, TX, USA
tara.s.radke@nasa.gov

Michael Bernatovich
Johnson Space Center
National Aeronautics and Space Administration
Houston, TX, USA
michael.a.bernatovich@nasa.gov

***Abstract*—The Orion Crew Module Uprighting System is a set of five airbags that are responsible for the uprighting of the crew module in the case of an inverted splashdown. A series of tests during the Underway Recovery Test 7 (URT-7) were run in preparation for the Artemis I mission, where the dynamic characterization of the CMUS in an ocean wave environment was performed. A Datawell Waverider DWR-G4 wave buoy was deployed to the characterize the wave environment during these tests. The heave measurements from this buoy were projected to the Orion Crew Module Buoyancy Test Article location by two different methods: (1) directly time-shifting the data, and (2) performing a frequency-domain, phase-shifting operation. Results demonstrate that the phase-shifting operation led to better correlation with the true crew module response to wave excitation as compared with the purely time-shifted method. Additionally, a novel approach to localize an object in a bidirectional wave field based on its heave response is presented and validated with URT-7 data. Given a wave measurement device at a known location, one can estimate the relative distance to another object based solely off its heave response. Results show that if signals have sufficiently good correlation, this method can be used to estimate the relative separation between two objects in the same wave field.**

Keywords—linear wave theory, wave dynamics, dynamic stability

I. Introduction

The Orion Crew Module Uprighting System (CMUS) is a set of five air bags spaced 60° apart that are responsible for the uprighting of the Orion Crew Module (CM) after it has landed in the ocean. Launch and re-entry constraints restrict the form of the outer mold line of the CM, resulting in a configuration with multiple stable orientations while floating in the water. The desired orientation is for the CM to be upright in the "Stable 1" orientation, while undesirable orientations are the nose-down configuration designated "Stable 2" (shown in Fig. 1) or a sideways configuration designed "Stable 3" (not shown). Inverted or sideways stable configurations for the CM would result in submergence of the hatch doors and communications antennae and an undesirable crew orientation. The CMUS provides the CM with additional buoyancy to reorient itself into the upright configuration post-splashdown and maintain this orientation for at least 24 hours. A depiction of the uprighting event on a 1/4 scale test article is shown in Fig. 2.

During the Apollo, Skylab, and Apollo-Soyuz programs, 47% of all landings resulted in an inverted orientation, with the nose of the crew module submerged – creating a risk to crew egress [1-17]. Additionally, the Stable 2 orientation complicated recovery operations, with the recovery team losing contact with the crew module due to submerged or partially submerged antennae [3]. In the Apollo-Soyuz rendezvous mission recovery, it is suspected that the Stable 2 orientation led to a salt water leak that shorted the communication line, ultimately preventing the recovery team from communicating with the crew [16]. The CMUS seeks to address these risks and upright the CM prior to the arrival of the recovery team, and remaining in the Stable 1 orientation for 24 hours.

Recently, testing has been performed to characterize the dynamic response of the CM during seakeeping and uprighting.

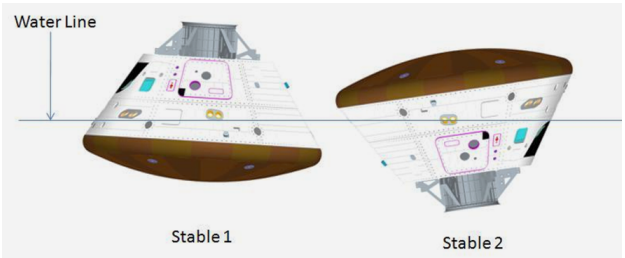

Fig. 1. The Orion CM in the desired, "Stable 1," configuration with crew access hatch accessible (left), and the undesired, "Stable 2," orientation with antennae and crew hatch submerged (right).

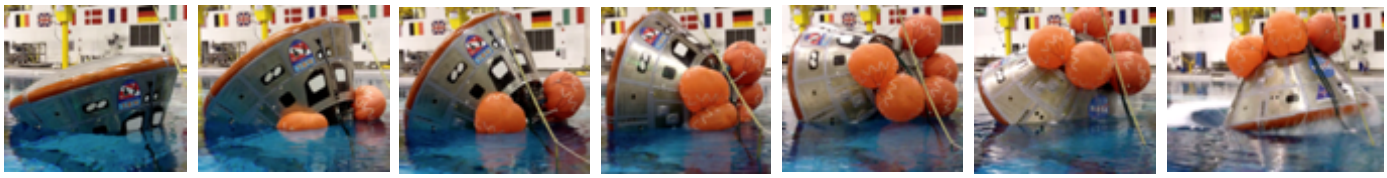

Fig. 2. 1/4 scale Orion Buoyancy Test Article (BTA) uprighting at the Neutral Buoyancy Lab (NBL) at Johnson Space Center. During this test, the five airbags inflated to upright the BTA from an undesirable Stable 2 orientation to the desirable Stable 1 orientation.

The main objective of this paper is to present the results from the seakeeping portions of Underway Recovery Test 7 (URT-7), including a novel approach to locate an object using its heave response and the heave response of a second object whose location is known. This novel localization method is developed in support of other Orion open water tests, where a GPS telemetry may not be available. For URT-7, an external wave measurement device (Datawell Waverider DWR-G4 buoy) was used to characterize the wave excitation around CM buoyancy test article (BTA). This is intended to provide both statistical and time-domain ocean wave characteristics projected to the location of the BTA, which are combined with the motion of the CM test article to evaluate the response of the CM to known input conditions. This is used to tune model parameters and validate dynamic simulations of the uprighting event for the range of waves observed during the test campaign.

This paper is structured as follows: Section II presents background information on the Orion Multi-purpose Crew Vehicle (MPCV) and the CMUS, along with the design and performance of the historical Apollo Command Module Uprighting System (ACMUS). Section III introduces the mathematical concepts behind the analysis and presents a novel method of locating an object in a bidirectional wave spectrum, using the heave response at a known location. Section IV describes the concept of operations and instrumentation used in URT-7. Section V presents the analysis of the URT-7 data. Section VI closes this work with some concluding remarks.

II. Background

This section presents background on the Orion CMUS and a historical perspective of the design and performance of the Apollo Command Module Uprighting System.

A. Artemis I and Artemis II

The CMUS characterization effort described in this work is performed in support of the Artemis moon program. The first launch of the Artemis program will be the Artemis I mission, an uncrewed lunar orbital test flight, currently slated to launch in mid to late 2020. Artemis I will be the maiden flight of the Space Launch System heavy lift launch vehicle and the Orion crew module. Orion will be put in a 6-day lunar distant retrograde orbit around the moon, followed by a return to earth, with a landing in the Pacific Ocean. The following mission, Artemis II, will be the first crewed mission of the Artemis program. Both Artemis I and Artemis II missions, as well as all future missions of the Artemis program, will utilize the CMUS to upright the crew module in the case of an inverted landing and maintain the stable upright configuration in waves.

B. Splashdown and Recovery

During a nominal re-entry for the Artemis I mission, the Orion CM will deploy three parachutes to decelerate the capsule before splashdown in the Pacific Ocean. After splashdown, the parachutes are released. It was found during the Apollo program that the delay between splashdown and parachute release was critical in determining whether the Apollo command module would invert into the Stable 2 orientation. Right after splashdown and before parachute release, Apollo crew members suspected that the wind loading on the parachutes was sufficient to overturn the Apollo command module [2] [3] [6] [7] [11]. After parachute release, if the Orion CM is in the Stable 2 orientation, the CMUS will activate to upright the CM. In the case of an off-nominal re-entry (e.g., an ascent abort), the CMUS is also required to maintain the static stability of the CM in the Stable 1 orientation for at least 24 hours while rescue and recovery crews proceed to the new splashdown location. Once recovery teams make it to the CM, a collar is installed to assist in maintaining the CM upright during transit to the well deck of an amphibious transport ship. Winch lines are installed, and the CM is towed to the well deck and fit into a cradle [18].

TABLE I. Apollo, Skylab, and Apollo-Soyuz Missions Splashdown and Landing Oreintations

Mission	Stable 1	Stable 2
AS-201	X	
AS-202	X	
Apollo 4	X	
Apollo 6		X
Apollo 7		X
Apollo 8		X
Apollo 9	X	
Apollo 10	X	
Apollo 11		X
Apollo 12		X
Apollo 13	X	
Apollo 14	X	
Apollo 15	X	
Apollo 16		X
Apollo 17	X	
Skylab 2	X	
Skylab 3		X
Skylab 4		X
Apollo-Soyuz		X

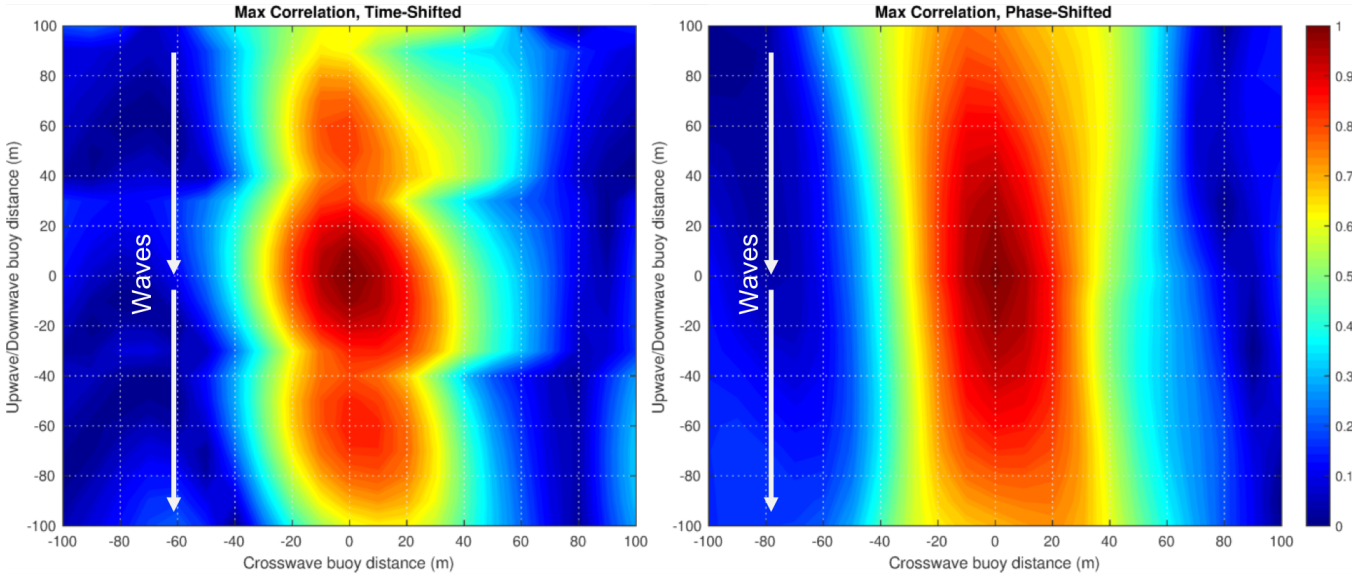

Fig. 3. Maximum cross-correlation coefficient at different distances from measurement source at (0,0) under northerly waves. On the left, a cross-correlation is directly applied between the two signals (a). On the right, the phase-shifting operation as described in Section III.A is applied before the cross-correlation is calculated. There is a larger area with more correlation in (b) when compared to (a). Thus, applying a phase-shifting of the heave signal from the DWR-G4 will produce a more accurate estimate of the wave environment at the BTA location.

C. Apollo Uprighting System Design and Performance

Similar to CMUS, the Apollo Command Module Upright System (ACMUS) was a set of three airbags responsible for the uprighting of the Apollo command module. Roughly half of all Apollo landings resulted with the command module inverted in the Stable 2 orientation. Table 1 breaks down the landing orientation for every flight of the Apollo command module. For every Stable 2 landing, the ACMUS successfully uprighted the capsule, allowing the recovery team to safely extract the crew.

There are a number of differences between Orion's CMUS and the ACMUS. Due to Orion's larger diameter as compared to the Apollo command module, five airbags are required to upright Orion, whereas the smaller Apollo command module only required three airbags. The Apollo airbags were inflated using a compressor and solenoid valves, while the CMUS uses pyro-valves and helium to inflate the airbags. As a result, the CMUS inflation system is lighter than the ACMUS system. The design philosophy also differs between the two. The ACMUS emphasized testing, with over 100 uprighting tests occurring throughout the design. The CMUS emphasizes a stronger modeling approach and includes a smaller number of tests.

III. Mathermatical Modeling of Wave Dynamics

The process of projecting a wave train from an external wave measurement device to a location of interest is described in this section. This approach was taken to estimate the wave environment around the BTA for the URT-7 test. During the URT-7 test, a DWR-G4 wave buoy was used as the external measurement device to capture the heaving motion induced by waves near the Buoyancy Test Article (BTA). It was necessary to project the wave train from the buoy location to the BTA location. Assuming a wave spectrum that does not vary with time, one can perform a *phase-shifting* of the wave dynamics in the frequency domain to collocate the wave buoy heave response to the desired location (i.e., the CM BTA location). The wave excitation at the BTA location is used as an input to modeling and simulation software. A comparison can then be made between the modeled BTA response in simulation and the true response from URT-7 data.

A. Projection of Wave Train to External Location

Assuming small amplitude linear gravity waves, the heave motion of the wave, η, at location (x, y) and time t can be modeled as a summation [19],

$$\eta(x,y,t) = \sum_{\ell} A_{\ell} \cos\left(k_{\ell x}x + k_{\ell y}y - \omega_{l}t - \phi\right), \quad (1)$$

where ω_l is the frequency of a wave, ϕ is the phase of the wave, and $k_{\ell x}$ and $k_{\ell y}$ are the directional wave numbers in the x and y axes, respectively, for wave element ℓ. Assuming deep water waves, the wave number k can be approximated as,

$$k_{\ell} \approx \omega_{\ell}^2/g, \quad (2)$$

where g is the gravitational acceleration term. The directional wave numbers are modeled as,

$$k_{\ell x} = k_{\ell}\cos\theta, \quad (3)$$

$$k_{\ell y} = k_{\ell}\sin\theta, \quad (4)$$

where θ is the angle of the propagating wave defined relative to a chosen frame.

The main objective is to project a wave train from an external measurement device to a desired location. This can be accomplished by transforming the wave heave motion in (1) into the frequency domain and applying a phase-shift on a per wave-element basis, as determined by the relative separation of the external measurement device and the location of interest. Let x_{sep} and y_{sep} be the relative separation of the location of interest and the measurement location. Assuming stationary, or nearly stationary, locations for both the measurement location

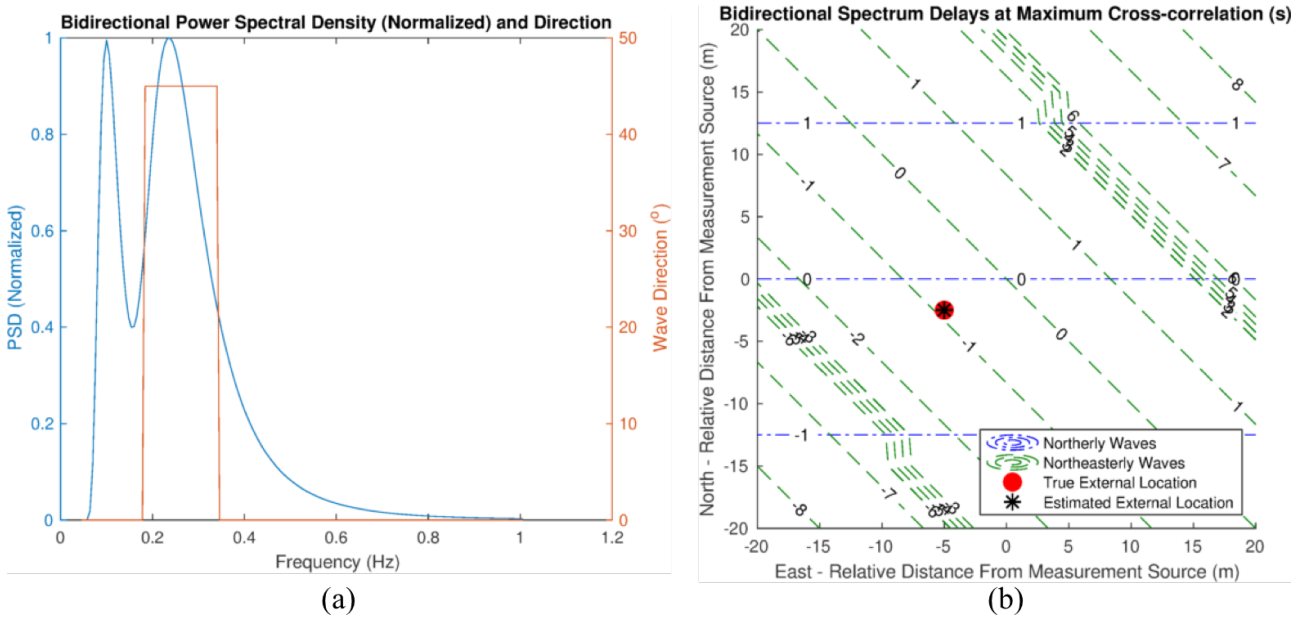

(a) (b)

Fig. 4. The bimodal, bidirectional spectrum power spectral density (PSD) and direction (a) and the time delay map for that spectrum (b). The blue line in (a) denotes the normalized PSD of the wave spectrum, and the redline depicts the direction. The mode centered around 0.1Hz is predominantly from the northern direction, while the lobe centered about 0.25Hz is predominantly from the northeastern direction. The red dot in (b) shows the true relative location of an external object, and the black asterisk (*) depicts the location estimate using the bidirectional localization technique proposed in Section III.C.

and the location of interest, one can set the origin of the inertial frame at the measurement location such that $x = 0$ and $y = 0$. The location of interest in this frame is $x = x_{sep}$ and $y = y_{sep}$.

A Fourier transform can be applied to (1), resulting in the following frequency domain representation of the wave heave motion signal, $\mathrm{H}(x, y, \omega)$, at location x and y:

$$\mathrm{H}(x,y,\omega) = \pi \sum_\ell A_\ell \exp\Big(i\big(\phi - k_{\ell x}x - k_{\ell y}y\big)\Big)\left[\delta(\omega-\omega_l)+\delta(\omega+\omega_l)\right], \quad (5)$$

where $i = \sqrt{-1}$ and δ is the Dirac delta function. The wave train can now be projected to an arbitrary location as defined by x and y. For the URT-7 analysis, the wave train is projected to $x = x_{sep}$ and $y = y_{sep}$. To reproduce the signal in the time domain at the new location, the inverse Fourier transform must be applied to (5).

B. Phase-Shifted Versus Time-Shifted Comparison

The phase-shifted approach can be compared against a less location-informed approach where the external heave measurements are *time-shifted* to match the CM location. Essentially, a lag (the *time-shift*) is applied such that the cross-correlation between the external heave measurements and the CM is maximized. This approach does not take into account any insights that linear gravity wave theory may offer, and as a result, suffers from poorer correlation.

Defining a *cosine-n* directional Bretschneider spectrum as [20],

$$F_{dir}(\theta) = \frac{2}{\pi}\cos^{2n}(\theta), \quad (6)$$

$$F(\omega,\theta) = F_{dir}(\theta)\frac{1.25}{4}\frac{\omega_m^4}{\omega^5}\zeta^2 e^{-1.25\left(\frac{\omega_m}{\omega}\right)^4}, \quad (7)$$

where $F(\omega, \theta)$ is the directional power spectral density of the wave spectrum for a given frequency ω and direction θ, where ω_m is the peak wave frequency and ζ is the peak wave height. The directional spreading of the wave spectrum is defined by the *cosine-n* term in (6), where n defines the spreading factor. As an example, a northerly wave (i.e., $\theta = 0^o$) is simulated with a peak wave height $\zeta = 1$ m, peak frequency $\omega_m = 1/7$Hz, and spreading factor $n = 4$. The heave signal at various locations is calculated using (1). A normalized cross-correlation coefficient is calculated between the signal at the origin (x_0, y_0) and at an arbitrary location (x_1, y_1) as [21],

$$r = \frac{E[\{\eta_0(x_0=0,y_0=0,t)\}\{\eta_1(x_1,y_1,t)\}]}{\sigma_{\eta_0}\sigma_{\eta_1}}, \quad (8)$$

where the E denotes the expectation of the signal, and σ_{η_0} and σ_{η_1} are the standard deviations for η_0 and η_1, respectively. It should be noted that the means of both η_0 and η_1 signals are zero.

The contour maps in Fig. 3 denote the differences in the maximum correlation coefficient between the time-shifting and phase-shifting approach. The cross-correlation is calculated relative to a measurement source at the origin. For the field trials described in this work, the external wave measurement device, the DWR-G4, was left to free drift around CM. A key objective was to maximize the correlation between the projected wave train, as calculated from the DWR-G4, to the actual wave train at the CM location. Since both CM and DWR-G4 are free-drifting and will move relative one another, it was desirable to maximize the area around the CM where the correlation coefficient was highest. The phase-shifting approach consistently outperformed the time-shifting approach in terms of area with the highest correlation coefficients.

C. Bidirectional Spectral Localization

In this section, an inverse approach is taken. Instead of using the relative separation between a measurement device and location of interest to increase the maximum cross-correlation of the signals by *phase-shifting* one of them, the relative separation is estimated by examining the cross-correlation of the signals. A novel process of locating an object based solely off its response in a bidirectional wave field is presented here. The key requirement is that the two directions in the spectrum be sufficiently separated in frequency. Although only a bidirectional wave field is considered, this application can be extended to an arbitrary number of wave directions, further increasing the accuracy of the resultant location estimate. It is assumed that the location of one of the objects is known. Using the heave motion at this location, one can estimate the relative separation of another object in the same wave field solely by the heave response of the second object. For the URT-7 test, the object with the known location is taken to be the DWR-G4 wave buoy. The second object whose position is to be estimated is the BTA. This process is presented here primarily in support of other open-water CMUS tests, where location information of the BTA relative to the wave measurement buoy may not be available.

Consider two objects in a wave field of sufficiently long wavelengths that cause both objects to follow the heaving motion of the wave, without exciting additional dynamics (e.g., rolling and pitching responses). Under these conditions, both bodies will act like buoys and "ride" the wave crests and troughs. A bidirectional spectrum is simulated using (6) and (7), with one wave field coming in from a northerly direction ($\theta = 0^o$) and a second wave field coming in from a northeasterly direction ($\theta = 45^o$). The power spectral density and direction of these wave fields are depicted in Fig. 4a. Much like the cross-correlation coefficient maps in Fig. 3, one can construct a contour map of the time delay τ associated with the maximum cross-correlation coefficient, relative to a signal measured at the origin. One can bandpass filter the heave signal at each location to separate the effects of both wave fields, and construct a time delay contour map for both. An example contour map using the wave fields defined previously is found in Fig. 4b. The dashed and dashed-dotted lines connect locations with the same time delay. It is apparent that the contour lines from the northerly wave field and the northeasterly wave field intersect at only one location. Thus, given the heave measurement at an arbitrary location, one can bandpass filter the signal to separate the responses from both wave fields, and calculate τ for each.

Consider the heave signal of an object at an unknown location. Let the time delay from the northerly wave field be τ_1 and the northeasterly wave field be τ_2. An optimizer can be constructed to estimate the object's location, $\hat{x}$ and $\hat{y}$, by examining the expected time delays from the measurement source, which, in this case, is taken to be at the origin. Using a maximum correlation coefficient time delay map as in Fig. 4b, a function $\mathrm{T}_i : \mathbb{R}^2 \to \mathbb{R}$ can be approximated that maps a location (x, y) to its corresponding delay for each wave field i. An objective function is defined as,

$$\min_{\hat{x},\hat{y}} J(\hat{x},\hat{y}), \tag{9}$$

$$J(\hat{x},\hat{y}) = \sqrt{(\tau_1 - \mathrm{T}_1(\hat{x},\hat{y}))^2 + (\tau_2 - \mathrm{T}_2(\hat{x},\hat{y}))^2}. \tag{10}$$

Effectively, the objective function tries to minimize the root-sum-square of the error between the measured time delay for each wave field and the optimizer estimate of the location. Once the minimum is found, the location estimate can be extracted from T_i. This optimization process is implemented on a nonlinear optimizer, such as *fmincon* in the MATLAB Optimization Toolbox.

An example of the efficacy of this localization method is presented in Fig. 4b, where the true location of the heave measurement is denoted by the red dot, and the estimated location is denoted by the black asterisk. It is clear that the localization method was successfully able to estimate the relative location of the object from the measurement device to within 10cm. It should be noted that this method relies on a bidirectional spectrum. If the wave field only has a single directional component, then only the "downwave" axis can be estimated with this approach – the "crosswave" axis would remain unknown.

IV. Underway Recovery Test 7

The Underway Recovery Test-7 (URT-7) was conducted between October 31, 2018 to November 4, 2018 off the southern coast of California. It was the seventh in a series of tests that exercised the recovery of the Orion CM, evaluating processes, procedures, hardware, and personnel. The URTs are a joint effort between NASA Exploration Ground Systems and the U.S. Navy to fully validate the Orion CM recovery process. For the URT-7 test, a San Antonio-class amphibious transport ship, the USS John P. Murtha, was used to retrieve an Orion buoyancy test article from open water. The well deck of the John P. Murtha, originally designed to launch and recover amphibious craft, was used to capture the Orion BTA. While the BTA was in open water, a wave buoy, the Datawell Waverider, DWR-G4, was deployed 50m upstream of the BTA

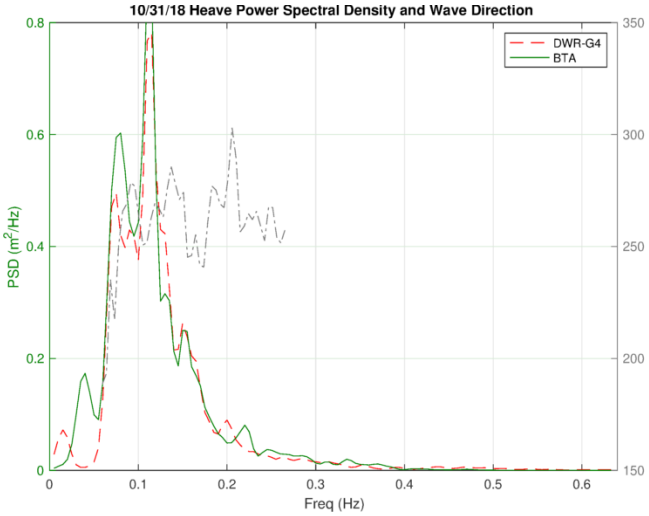

Fig. 5. The calculated BTA (green) and DWR-G4 (green) wave spectral density for the 10/31/2018 test date for URT-7. The wave direction as calculated from the DWR-G4 is shown in gray. Although both devices used fundamentally different mechanisms – the DWR-G4 used the doppler shift of the GPS signals and the BTA used a piezoelectric MEMS accelerometer – both produced similar results with a peak wave concentrated at 0.11Hz.

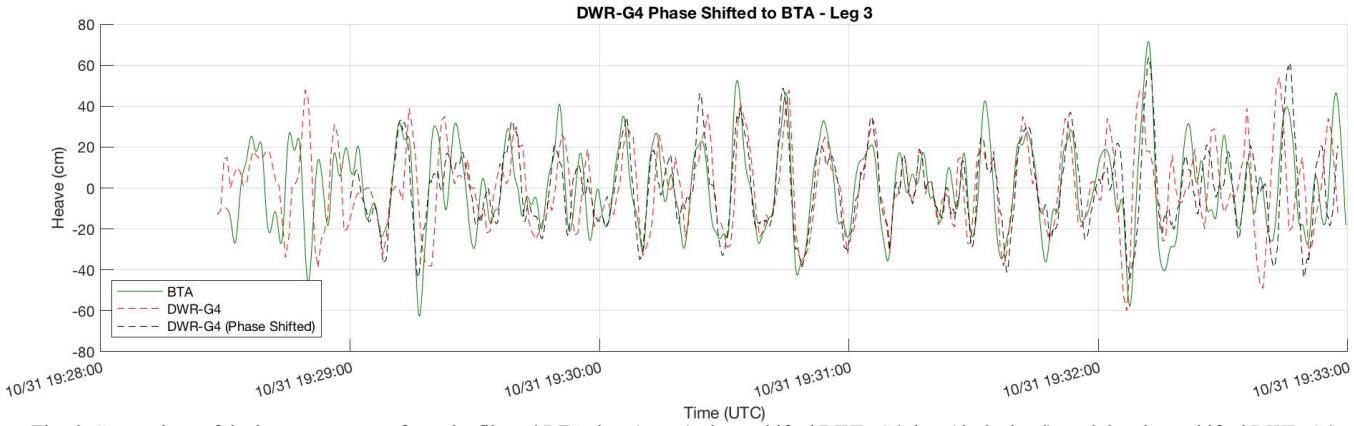

Fig. 6. Comparison of the heave responses from the filtered BTA data (green), the unshifted DWR-G4 data (dashed red), and the phase-shifted DWR-G4 at the BTA location (dashed black). It is evident that the phase-shifted DWR-G4 heave response is a closer match to the actual heave response of the BTA.

to characterize the wave environment. This was used to judge the seakeeping characteristics of the CM. These two objects were left to free-drift, and the DWR-G4 was redeployed after it exceeded a 50m downwave distance from the BTA, or 35m crosswave distance. A Rigid Hull Inflatable Boat (RHIB) was used to deploy and recover the DWR-G4, as well as to retrieve and re-deploy the buoy to ensure the proximity of the wave buoy to the BTA fit into the dumbbell shape of the desired measurement area, as depicted in Fig. 7.

A. Instrumentation

A DWR-G4 wave buoy was used to record wave measurements "upwave" and "downwave" of the CM. The DWR-G4 is one-meter diameter wave buoy produced by Datawell BV. The wave buoy is instrumented with a GPS, capable of measuring both the location of the buoy and the buoy response to waves. The heaving, surging, and swaying motion of the buoy on the free surface of the water causes small shifts in the frequency of the GPS signal. The buoy uses the doppler frequency shift of this signal to calculate the wave height and direction in its immediate environment. The DWR-G4 is capable of producing both wave spectral information as well as time histories of its surging, swaying, and heaving motion. A wave spectrum file with the power spectral density and wave direction was logged every 30 minutes. The time histories of the heave, surge, and sway measurements were logged in 30 minute segments at 1.28Hz. Internal filtering of the DWR-G4 produced an estimate of the heave, surge, and sway motion between 0 and 0.4Hz. A phase shifting operation, as described in Section III.B, was applied to the raw time histories to project the local wave environment from the DWR-G4 to the BTA. The spectral information was used in the statistical analysis of the wave environment.

In addition to the onboard GPS on the DWR-G4, an external GPS was attached to a collar around the buoy. The DWR-G4 is designed to be moored to single location and only logs its GPS location infrequently. The external GPS was capable of logging GPS locations at up to 1/7 Hz to an external storage device. Only the external GPS measurements were used for localization of the wave buoy – the internal GPS was used solely for wave characterization.

The BTA was outfitted with an Xsens MTi-G700 GPS-aided inertial measurement unit (IMU). The MTi-G700 instrument included a three-axis gyroscope, a three-axis accelerometer, a three-axis magnetometer, and a GPS. The measurements from each of these devices are Kalman filtered to produce a state estimate. Kalman filter coefficients can be configured, dependent on the relevant dynamics being measured. Both filtered data and raw data from each individual sensor was logged by a support computer. For the post-processing of the URT-7 data, only the raw accelerometer data and GPS data were analyzed. The raw accelerometer data were bandpass filtered and integrated to produce a heave estimate of the BTA, while the GPS data were used to calculate the relative separation between the DWR-G4 and the BTA.

Personnel on the RHIB used a laser rangefinder to determine the separation between the BTA and the DWR-G4. Once that separation exceeded approximately 50 m downwave, the DWR-G4 was repositioned 50 m upstream of the BTA.

B. URT-7 Wave Characterization Concept of Operations

The wave characterization effort during URT-7 occurred separately from the recovery operations. The USS John P. Murtha was positioned far outside, and downwave, of the operational area with the BTA and wave buoy. A remote team

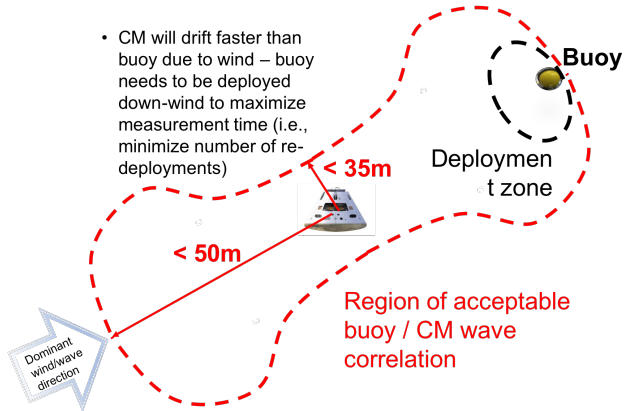

Fig. 7. The desired mission area was set to maximize the cross-correlation between the CM and DWR-G4 heave signals using the phase-shifting operation in Section III.A. This resulted in a "dumbbell" shape as shown above.

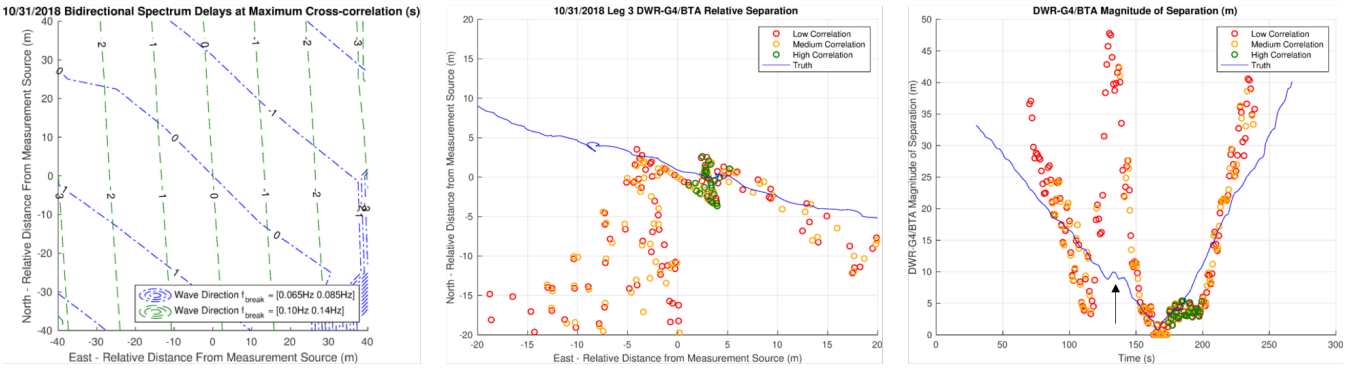

(a) (b) (c)

Fig. 8. The bidirectional localization method efficacy for the wave field in (a). A map of the estimated position (circles) versus the true position (blue line) is shown in (b). The magnitude of the separation is given in (c). Both (b) and (c) break down estimates into time points with high (green), medium (yellow), and low (red) correlation coefficients. An anomaly at 130s lowered the cross-correlation between the signals and produced a poor location estimate, as denoted by the black arrow in (c). A potential explanation for the anomaly is the passing wake from the RHIB.

was stationed on the ship and monitored telemetry from the DWR-G4 through an ARGOS satellite link. The RHIB was staffed with Navy personnel who were responsible for deploying and recovering the wave buoy.

The phase-shifting analysis presented in Section III.B was used to inform the deployment of the wave buoy relative to the BTA. As one can see from Fig. 3b, the area with the largest amount of correlation is approximately +/-70m downwave and +/-35m crosswave from the location of interest. To simplify operations, the maximum distance established was 50 m. The RHIB crew deployed the DWR-G4 at the BTA location and let it drift until the separation distance reached 50 m before retrieving it and redeploying it 50 m on the opposite side of the BTA for the duration of the test. To assist with the repositioning of the DWR-G4, the crew used a laser range finder to find the separation between the BTA and the DWR-G4. Both BTA and DWR-G4 were left to free-drift to obtain heave measurements. The drift speed of both was under 0.3 m/s, which did not contribute significantly to the frequency shift of the wave spectral content. The repositioning of the wave buoy discretized the data set into discrete segments. These segments are referred to as "legs" in this work, and varied from five to eight minutes in duration.

V. Underway Recovery Test 7 Results

This section presents the results from post-processing the data from the URT-7 wave characterization effort. For the URT-7 data sets, only long period waves with correspondingly low frequencies were present. This caused both the DWR-G4 and the BTA to behave like wave buoys – "riding" the crests and troughs of waves. Wave spectral data demonstrated that the peak wave amplitude was not high enough to excite BTA rolling and pitching dynamics, and there was ample frequency separation between the peak wave frequency and the expected dynamics of the BTA.

A. BTA Heave Measurements and Wave Spectral Content

Since the BTA was outfitted with the MTiG-700 IMU, it was possible to calculate its heave response using the onboard accelerometer. A sixteenth-order Butterworth bandpass filter was applied to the raw accelerometer data to filter only the frequencies of interest from 1/30 Hz to 2 Hz. This was then integrated twice to obtain the vertical displacement of the BTA. Performing the same discrete Fourier transform process as the DWR-G4 produced the wave spectral content.

In comparison, the heave time history output of the DWR-G4 already filtered the results to the frequency range of interest. It was straightforward to apply a discrete Fourier transform to extract the frequency content of the signal. Likewise, the wave direction could be calculated using all three heave, surge, and sway time histories. The full process to calculate the wave direction is out of scope for this work, but can be found in [22].

Fig. 5 shows the comparison between the power spectral density as calculated from the DWR-G4 (red) and the BTA accelerometer (green) for the 10/31/2018 test date. It should be noted that even though the DWR-G4 and the BTA used fundamentally different sensors to determine the wave spectral content both produced similar power spectral densities, with most of the peak wave frequency concentrated at 0.11 Hz. The lack of content at higher frequencies in the BTA PSD shows that the wave environment was not sufficient to excite local BTA dynamics. Thus, both systems behaved like wave buoys. The test dataset from URT-7 is a good candidate to validate the phase-shifting approach in Section III.A and the bidirectional localization technique presented in Section III.C.

B. Efficacy of Phase-Shifting Wave Train to BTA Location

Although the BTA was able to provide an adequate measurement of the wave environment in its immediate surroundings due to the relatively low peak wave frequency, it was still necessary to project the heave measurements of the DWR-G4 to the BTA. This is used primarily as a verification of the phase-shifting approach to support other Orion BTA open-water tests, which may not exhibit as benign of a wave environment, or during uprighting, where local BTA dynamics would be exercised.

Using the DWR-G4 heave time history, it was straightforward to apply the phase-shifting technique described in Section III.A. In this application, the location of interest was the BTA, and the known location was the DWR-G4. Fig. 6 displays a representative example from the third "leg" of the 10/31/2018 test date. The post-processed BTA heave response (green) is compared against both the unshifted and phase-

shifted DWR-G4 heave response (dashed red and dashed black, respectively). At the start of the leg, the buoy was upwave from the BTA, with the wave train first exciting the BTA, followed by the DWR-G4 a short time later. After two and a half minutes, at 19:30:30 UTC, the buoy comes within a short distance of the BTA, and both exhibit nearly identical heave excitation. The environment then moves the buoy upwave of the BTA, before leaving the designated operational area and being repositioned by the RHIB team. Throughout the leg, the phase-shifted buoy response was able to more accurately replicate the BTA heave response, demonstrating the efficacy of the phase-shifting. The phase-shifted response was also able to replicate the large heave motions exhibited by the BTA at 19:29:20 and 19:32:10 UTC.

C. Efficacy of the Bidirectional Localization

During the URT-7, the wave field was strongly monodirectional, with prominent westerly waves during all three test days. This proved to be a difficult validation of the bidirectional localization approach presented in Section III.C. However, some important insights could still be gleaned from the application of this process.

The power spectral density and wave direction from the 10/31/2018 test date is found in Fig. 5. It is clear that the waves were predominantly monodirectional but there was a slight southerly component in the lower frequency spectrum below 0.1 Hz that could be used to perform the bidirectional analysis. A low frequency passband and a high frequency passband were defined between 0.065 and 0.085Hz; and 0.10 and 0.14Hz, respectively. This roughly segmented out the two distinct peaks in the wave spectral content at 0.07 Hz and 0.11 Hz. The cross-correlation delay contour map is given in Fig. 8a.

The bidirectional localization process as described in Section III.C was applied to the bandpass filtered signals. A windowed cross-correlation was applied to account for the relative drift between the BTA and the DWR-G4. The lags associated with the maximum cross-correlation of the low and high frequency signals were used to localize the BTA with respect to the DWR-G4. The results are depicted in Fig. 8b and Fig. 8c, broken down by time points with high (red), medium (yellow), and low (red) cross-correlation. It is clear that during portions of the test where the correlation was the highest, there was an accurate estimate of their separation – within a meter for some time points. As the correlation between these two signals decreased, there were worse estimates, particularly in the BTA cross-track direction. However, when ignoring the directionality and examining only the magnitude of separation, most time points were able to adequately produce an estimate regardless of the associated correlation at that time point. There was an anomaly at 130s that was present in both truth and estimated data, as shown by the black arrow in Fig. 8c. This created a poorly correlated signal, and lead to a corresponding poor estimate of the BTA/DWR-G4 separation. A possible explanation for the anomaly is the effect of a wake from a passing boat, potentially from the RHIB craft. Excluding this portion of the data, the bidirectional localization was able to characterize the magnitude of the separation to within 10m, even for poorly correlated signals.

There are a number of reasons for the underperforming location estimates during the URT-7 test. The first is that the waves were strongly monodirectional, and did not have a large differentiation in frequency in the bimodal response. The second is the short time history of the DWR-G4 heave, surge, and sway response. This led to a noisy wave direction estimate. Despite these challenges, a location estimate of the BTA was produced with only five minutes of data, or roughly, only 400 sample from the DWR-G4. Additionally, the magnitude of the relative distances was accurately calculated with the exception of an anomalous event occurring 130s into the test.

VI. Conclusion

In this work, the results from the URT-7 were presented. Although the objectives for URT-7 were primarily to exercise the Orion CM recovery process, valuable ocean wave environment data were collected and correlated with free-floating BTA motions. A DWR-G4 wave buoy was deployed within 50 m of the Orion BTA to obtain heave measurements, which were then phase-shifted to the Orion BTA location. Since the wave spectral content was not in the frequency range of the local BTA dynamics, both DWR-G4 and BTA acted like "wave buoys" under long period waves. This allowed the phase-shifting process to be validated with the heave measurements from the DWR-G4 IMU. Results demonstrated that the phase-shifting process produced better correlation to the true BTA heave measurements than the time-shifting process. Additionally, a novel method for locating an object using solely its heave measurements under sufficiently long waves was presented and validated using URT-7 data. Results were mixed due to the poor frequency separation of the bimodal spectrum, the low number of samples introduced noise in the wave direction calculations, and the strongly monodirectional wave content. However, strongly correlated portions of each test were able to locate the BTA relative to the wave buoy within 10m. This provides a method for producing a rough estimate of the buoy-BTA separation for scenarios where BTA position data is not available.

Forward work will include post-processing of Uprighting Tests performed in the Atlantic, a recent validation of the uprighting process of the CMUS. The Atlantic Test validated CMUS operations in wind driven sea under various failure modes (e.g. only 4 of the 5 bags inflated). The DWR-G4 wave buoy was free drifting before, during, and after the uprighting event. The phase shifted correlation presented here will allow for the posttest analysis of CMUS during uprighting. Additionally, the field test data collected during URT-7 and the Atlantic Uprighting test will be used to validate the seakeeping and uprighting models being develop to support the CMUS system.

VII. Works Cited

[1] Office of Manned Space Flight, "Final Flight Evaluation Report Apollo 6 Mission," National Aeronautics and Space Administration, Houston, Texas, USA, 1969.

[2] Manned Spacecraft Center, "Apollo 7 Mission Report," National Aeronautics and Space Administration, Houston, Texas, USA, 1968.

[3] Manned Spacecraft Center, "Apollo 8 Mission Report," National Aeronautics and Space Administration, Houston, Texas, USA, 1969.

[4] Manned Spacecraft Center, "Apollo 9 Mission Report," National Aeronautics and Space Administration, Houston, Texas, USA, 1969.

[5] Manned Spacecraft Center, "Apollo 10 Mission Report," National Aeronautics and Space Administration, Houston, Texas, USA, 1969.

[6] Manned Spacecraft Center, "Apollo 11 Mission Report," National Aeronautics and Space Administration, Houston, Texas, USA, 1969.

[7] Manned Spacecraft Center, "Apollo 12 Mission Report," National Aeronautics and Space Administration, Houston, Texas, USA, 1970.

[8] Manned Spacecraft Center, "Apollo 13 Mission Report," National Aeronautics and Space Administration, Houston, Texas, USA, 1970.

[9] Manned Spacecraft Center, "Apollo 14 Mission Report," National Aeronautics and Space Administration, Houston, Texas, USA, 1971.

[10] Manned Spacecraft Center, "Apollo 15 Mission Report," National Aeronautics and Space Administration, Houston, Texas, USA, 1971.

[11] Manned Spacecraft Center, "Apollo 16 Mission Report," National Aeronautics and Space Administration, Houston, Texas, USA, 1972.

[12] Lyndon B. Johnson Space Center, "Apollo 17 Mission Report," National Aeronautics and Space Administration, Houston, Texas, USA, 1973.

[13] Lyndon B. Johnson Space Center, "Skylab Mission Report First Visit," National Aeronautics and Space Administration, Houston, Texas, USA, 1973.

[14] Lyndon B. Johnson Space Center, "Skylab Mission Report Second Visit," National Aeronautics and Space Administration, Houston, Texas, USA, 1974.

[15] Lyndon B. Johnson Space Center, "Skylab Mission Report Third Visit," National Aeronautics and Space Administration, Houston, Texas, USA, 1974.

[16] Lyndon B. Johnson Space Center, "Apollo Soyuz Mission Evaluation Report," National Aeronautics and Space Administration, Houston, Texas, USA, 1975.

[17] Manned Spacecraft Center, "Apollo Experience Report - Command Module Uprighting System," National Aeronautics and Space Administration, Houston, Texas, USA, 1973.

[18] John F. Kennedy Space Center, "NASA Facts: Orion Recovery Operations," National Aeronautics and Space Administration, Kennedy Space Center, FL, USA, 2018.

[19] R. G. Dean and R. A. Dalrymple, Wave Wave Mechanics for Engineers and Scientists, Singapore, Singapore: World Scientific Publishing Co. Pte. Ltd., 2010.

[20] M. St. Dinis and W. J. Pierson, "On the motions of ships in confused seas," New York Univ Bronx School of Engineering and Science, New York City, NY, USA, 1953.

[21] W. J. Emery and R. E. Thomson, Data Analysis Methods in Physical Oceanography, Amsterdam, The Netherlands: Elsevier B.V., 2004.

[22] Datawell BV Oceanographic Instruments, "Datawell Waverider Reference Manual," Datawell BV Oceanographic Instruments, The Netherlands, 2018.